Supplement 2

Table of Contents

List of S:CORT Investigators

Richard Adams (Cardiff University and Velindre Cancer Centre, Cardiff, UK)
Andrew Beggs (University of Birmingham, Birmingham, UK)
Louise Brown (University College London, London, UK)
Francesca Buffa (University of Oxford, Oxford, UK)
Enric Domingo (University of Oxford, Oxford, UK)
Andrew Blake (University of Oxford, Oxford, UK)
Chieh-His Wu (University of Southampton, Southampton, UK)
Aikaterini Chatzipli (Wellcome Sanger Institute, Hinxton, UK)
Susan Richman (University of Leeds, Leeds, UK)
Philip Dunne (Queen's University Belfast, Belfast, UK)
Chris Holmes (University of Oxford, Oxford, UK)
Denis Horgan (European Alliance for Personalised Medicine, Brussels, Belgium)
Rick Kaplan (University College London, London, UK)
Mark Lawler (Queen's University Belfast, Belfast, UK)
Simon Leedham (University of Oxford, Oxford, UK)
Tim Maughan (University of Oxford, Oxford, UK)
Ultan McDermott (Wellcome Sanger Institute, Hinxton, UK)
Gary Middleton (University of Birmingham, Birmingham, UK)
Dion Morton (University of Birmingham, Birmingham, UK)
Graeme Murray (University of Aberdeen, Aberdeen, UK)
Phil Quirke (University of Leeds, Leeds, UK)
Manuel Salto-Tellez (Queen's University Belfast, Belfast, UK)
Leslie Samuel (NHS Grampian, Aberdeen, UK)
Anna Schuh (University of Oxford, Oxford, UK)
David Sebag-Montefiore (University of Leeds, Leeds, UK)
Matt Seymour (University of Leeds, Leeds, UK)
Richard Sullivan (Kings College London, London, UK)
Ian Tomlinson (University of Edinburgh, Edinburgh, UK)
Nicholas West (University of Leeds, Leeds, UK)
Richard Wilson (University of Glasgow, Glasgow, UK)

Acknowledgements

The stratification in colorectal cancer consortium (S:CORT) is funded by a UK Medical Research Council (MRC) Stratified Medicine Consortium programme grant (grant ref MR/M016587/1) and co-funded by Cancer Research-UK. Additional funding support was received from the Ludwig Cancer Research Foundation. This study was not funded by the National Institutes of Health and no authors are employed by or a recipient of a grant from the National Institutes of Health.

List of Sites Enrolling in New EPOC

Surgical Site	Site Name	PI Name	Number of patients
Sheffield Teaching Hospitals NHS Foundation Trust	Sheffield	Dr Joanne Hornbuckle	15
United Bristol Healthcare Trust (Bristol Oncology and Haematology Centre)	Bristol	Dr Stephen Falk	15
Southampton University Hospital NHS Trust	Southampton	Prof John Primrose	11
Basingstoke and North Hampshire NHS Foundation Trust (North Hampshire Hospital)	Salisbury	Dr Tim Iveson	9
Southampton University Hospital NHS Trust	Bournemouth	Dr Tamas Hickish	8
United Bristol Healthcare Trust (Bristol Oncology and Haematology Centre)	Yeovil	Dr Clare Barlow	8
King's College NHS Foundation Trust	Guy's & St Thomas's	Dr Paul Ross	6
Aintree University Hospitals NHS Foundation Trust (University Hospital Aintree)	Clatterbridge	Dr David Smith / Dr Nua Chan Ton	5
Pennine Acute Hospitals NHS Trust (North Manchester)	Christie	Dr Juan Valle	5
Basingstoke and North Hampshire NHS Foundation Trust (North Hampshire Hospital)	Basingstoke	Dr Charlotte Rees	4
King's College NHS Foundation Trust	Maidstone	Dr Mark Hill	4
Royals Free Hampstead NHS Trust	North Middlesex	Prof John Bridgewater	4
The Royal Marsden NHS Foundation Trust Downs Road, Sutton Surrey & Fulham Road London	Royal Marsden (Surrey)	Prof David Cunningham	4
United Bristol Healthcare Trust (Bristol Oncology and Haematology Centre)	Weston General Hospital (WSMare)	Dr Majorie Tomlinson	4
University College London Hospitals	University College London Hospital	Prof John Bridgewater	4
Royals Free Hampstead NHS Trust	University College London Hospital	Prof John Bridgewater	3
University College London Hospitals	Princess Alexandra, Harrlow (PAH)	Prof John Bridgewater	3
Basingstoke and North Hampshire NHS Foundation Trust (North Hampshire Hospital)	Bedford	Dr Sarah Smith	2
Basingstoke and North Hampshire NHS Foundation Trust (North Hampshire Hospital)	Heatherwood & Wexham Park	Dr Marcia Hall	2
Cardiff and Vale NHS Trust	Velindre	Dr Alison Brewster	2

Hammersmith	Charing Cross (Imperial)	Dr Susan Cleator	2
Nottingham University Hospitals NHS Trust	Nottingham	Dr Vanessa Potter / Dr Georgina Walker	2
Royal Surrey County Hospital	Royal Surrey	Dr Sharadah Essapen	2
Royals Free Hampstead NHS Trust	Princess Alexandra, Harlow (PAH)	Prof John Bridgewater	2
Royals Free Hampstead NHS Trust	Royal Free	Dr Astrid Mayer	2
Southampton University Hospital NHS Trust	Winchester	Dr Luke Nolan	2
Aintree University Hospitals NHS Foundation Trust (University Hospital Aintree)	Aintree	-	1
Aintree University Hospitals NHS Foundation Trust (University Hospital Aintree)	Christie	Dr Juan Valle	1
Aintree University Hospitals NHS Foundation Trust (University Hospital Aintree)	Pennine	Dr Derek O'Reilly	1
Aintree University Hospitals NHS Foundation Trust (University Hospital Aintree)	Southport & Ormskirk	Dr Nasim Ali	1
Barts and The London NHS Trust (St BartholomewÕs Hospital)	Barking	Dr Sherif Raouf	1
Barts and The London NHS Trust (St BartholomewÕs Hospital)	Barts	Dr Sarah Slater	1
Basingstoke and North Hampshire NHS Foundation Trust (North Hampshire Hospital)	Poole	Dr Tamas Hickish	1
Basingstoke and North Hampshire NHS Foundation Trust (North Hampshire Hospital)	Portsmouth	Dr Ann O'Callaghan	1
Belfast Health & Social Care Trust	Belfast City Hospital	Dr Colin Purcell	1
Cambridge University Hospital NHS Trust (Addenbrookes Hospital)	Cambridge (Addenbrookes)	Dr Charles Wilson	1
Cambridge University Hospital NHS Trust (Addenbrookes Hospital)	West Suffolk	Dr (Margaret) Anne Moody	1
Central Manchester and Manchester Children's University Hospitals (Manchester Royal Infirmary)	Christie	Dr Juan Valle	1
Hammersmith	St Marys (Imperial)	Dr Susan Cleator	1
Lothian Health Board (Edinburgh Royal Infirmary)	Lothian Edinburgh	Dr Ewan Brown	1
Royals Free Hampstead NHS Trust	Barking	Dr Sherif Raouf	1
Southampton University Hospital NHS Trust	Isle of Wight	Dr Christopher Baughan	1

Southend University Hospital NHS Foundation Trust	Southend	Dr David Tsang	1

Supplemental Methods

Specimen Characteristics and Assay Methods

For the discovery cohort, formalin-fixed paraffin-embedded (FFPE) specimens from hepatic resections were histologically reviewed by an expert pathologist.[1] Three spatially separated 2-mm punch biopsies of tumor-rich areas within each metastasis was obtained for each specimen. Nucleic acids were extracted using the RecoverAll Total Nucleic Acid Isolation Kit. RNA integrity and quantity was assessed using an Agilent 2100 Bioanalyzer. Ribosomal RNAs were removed using the Illumina Ribo-Zero rRNA Removal Kit. Reverse-stranded paired-end 75 base-pair sequencing libraries were constructed using Illumina Total RNA Stranded Kits. Subsequently, libraries were sequenced on a HiSEQ2500 machine. For miRNA expression profiling, 500 ng of total RNA was processed for biotin labeling and the biotin-labeled targets were hybridized to Affymetrix miRNA 4.0 Array Chips in an Affymetrix 640 hybridization oven. Arrays were washed and stained in an Affymetrix Fluidics Station 450 and the arrays were scanned using the Affymetrix GeneChip Scanner 3000 7G. CEL intensity files were generated using GCOS software.

For the validation cohort, as part of the S:CORT consortium, archival liver metastasis and primary tumor FFPE blocks at the time of surgical resection from the New EPOC clinical trial were profiled.[2,3] Briefly, tumor material was identified on an adjacent hematoxylin and eosin–stained slide for macrodissection. Total RNA was extracted from sequential 5-mm sections using the Roche High Pure FFPE Extraction Kit (Roche Life Sciences) and amplified using the NuGen Ovation FFPE Amplification System v3 (NuGen San Carlos). The amplified product was hybridized to the Almac Diagnostics XCEL array (Almac), a cDNA microarray-based technology optimized for archival FFPE tissue, and analyzed using the Affymetrix Genechip 3000 7G scanner (Affymetrix). Quality control metrics relating to monitor image quality, in vitro transcription, hybridization to the array, and RNA degradation were assessed prior to uploading to the S:CORT server, where further quality control was performed. Expression data was downloaded from a privately accessed cBioPortal repository from S:CORT. CEL files were processed using Affymetrix Array Power Tools (APT).

Neural Network Classifier Training for Molecular Subtyping

In the discovery cohort, a machine learning neural network classifier was trained to classify colorectal cancer liver metastases into one of three molecular subtypes (canonical, immune, and stromal) using mRNA and miRNA expression features. The reference standard for training the neural network classifier were the molecular subtypes previously published using the similarity network fusion (SNF) clustering algorithm in the discovery cohort.[1] Of importance, although molecular subtypes were ultimately associated with survival in our discovery set, the original SNF algorithm clustered tumors based only on molecular features and not survival outcomes.

For 93 patients in our discovery set, expression data was available for 17,162 mRNAs and 778 miRNAs. After principal component analysis (PCA), 400 mRNAs were selected based on having the highest PC1 and PC2 loadings. 41 miRNAs were also selected because they were present in both our discovery and validation expression datasets. Notably, the neural network classifier performed most accurately when utilizing both mRNA and miRNA features, with suboptimal accuracy when using either mRNA or miRNA alone. This is consistent with the original clustering-based approach to define molecular subtypes.[1] Only the combination of mRNA and miRNA expression identified prognostic subgroups, while using mRNA or miRNA alone did not. The discovery set was split into 60% of the samples to train the model and 40% to test model accuracy. Using the standardized Z-score of the 441 features (400 mRNAs and 41 miRNAs) as input, a neural network containing a single hidden layer of 35 neurons was trained. In this way, 100 total neural networks were trained using 100 random 60% (training) / 40% (testing) groupings of the discovery set to optimize the model performance.

In addition, to reduce the number of model input features while optimizing model accuracy, recursive feature elimination was performed, where input features that did not contribute significantly to the model accuracy were successively eliminated. Recursive feature elimination used a support vector machine (SVM) classifier to select the lowest number of features that maximized the F1 model score (which represents the harmonic mean

of the precision/positive predictive value and recall/sensitivity of a test). 5-fold cross-validation was used. The final neural network model contained 24 mRNAs and 7 miRNAs. 100 neural networks were again trained using 100 random 60% (training) / 40% (testing) splitting. Each model outputs the probability that a given sample corresponds to canonical, immune, or stromal subtypes. The subtype selected by each model was the subtype that had the highest probability. The overall subtype classification for each sample was the most frequent subtype chosen across the 100 neural network models.

Application of the Molecular Subtype Classifier in Validation Cohort

In the validation cohort, xCel CEL files were quantitated, RMA background normalized, and log2 transformed using APT version 2.11.4. Of 110,425 total xCel probesets, model input was limited to the probesets that corresponded to the 31 features (24 mRNAs and 7 miRNAs). If multiple probes corresponded to a gene of interest, the probe with maximum mean expression was selected. Each feature value was normalized across all samples to produce Z-scores. For each specimen, these standardized Z-scores for each of the 31 features served as model input into the trained 100 neural network models. As in the discovery cohort, the subtype selected for each model was the subtype with the highest probability. The overall molecular subtype assigned for each sample in the validation cohort was the most frequent subtype chosen across the 100 models. The "predicted molecular subtype" in the validation cohort was referred to as the "molecular subtype" for simplicity.

Robustness and internal consistency of the classifier was evaluated. Because the overall predicted molecular subtype for each specimen was the most commonly predicted subtype of the 100 neural network models, concordance across each of the 100 models could be assessed. A truly random (i.e. non-predictive) classifier would be expected to have 33.3% concordance across the 100 models.

When computing the molecular subtype of a liver metastasis (utilized for the primary statistical analyses), gene expression data from the liver metastasis alone was utilized as model input. To investigate if the signature's prognostic performance was specific to application in metastases only, the molecular subtypes were also predicted for corresponding primary tumors. In this case, model input for each patient was limited to gene expression data for the primary tumor alone. To compare the prognostic performance of consensus molecular subtypes (CMSs) with our study's metastasis subtypes, CMSs of both the liver metastases and primary tumors were also determined.[4] Finally, an exploratory analysis assessing any relationship between CMS of the primary tumor and molecular subtype of the liver metastasis was performed utilizing Fisher's exact test.

Single Sample Gene-Set Enrichment Analysis

To confirm that the neural network classifier accurately captured the molecular phenotype of the computed molecular subtypes within the validation cohort, a single sample gene-set enrichment analysis (ssGSEA) was performed using the EGSEA package in R and the Hallmark gene set database. For each gene feature, the probe with the maximum average signal was selected. A gene matrix was created with row names corresponding to the Entrez IDs and columns corresponding to the sample IDs. The EGSEA function egsea.ma was performed using the gene expression data and the algorithm method set to ssgsea. The ssgsea algorithm is an expansion of the GSEA algorithm.[5] In brief, for each sample the gene expressions were rank-normalized and the Empirical Cumulative Distribution Function (ECDF) was calculated for each gene in the pathway as well as all the remaining genes. An enrichment score for a given pathway was then calculated by integrating the differences between the ECDFs.

Immune Deconvolution

To additionally validate the molecular phenotype of predicted molecular subtypes in the validation cohort, immune deconvolution from the transcriptome was performed to estimate the presence of various immune cells in the tumor microenvironment. First, probeset level data was collapsed to gene level by taking the mean of the probesets. Then, absolute abundance of eight immune and two stromal features was generated with the R package, MCPcounter that provides a matrix table where each row corresponds to a feature and each column to a sample.[6]

Determination of Clinical Risk Score

The Clinical Risk Score (CRS) was developed by Fong et al and utilizes clinical and pathologic features to risk stratify patients undergoing hepatic resection for metastatic colorectal cancer.[7] Higher CRS is associated with worse survival after resection, and one point is awarded for a node-positive primary tumor, disease-free interval < 12 months, >1 metastatic tumor, preoperative CEA > 200 ng/ml, and size of largest metastasis > 5cm (maximum 5 points). In the original proposal of integrated clinical-molecular risk groups, the liver metastasis molecular subtypes were combined with CRS (≥2 or <2) to classify patients as low, intermediate, or high integrated risk.[1] Patients were excluded from analyses of integrated risk stratification if their CRS could not be classified as ≥ 2 or < 2. If a patient was missing one or more components of the CRS but the score was already 2 or greater, they were classified as having a high CRS (i.e. ≥2).

Supplemental Results

KRAS and *BRAF* Alterations and Microsatellite Instability

Among patients with evaluable mutation status, *KRAS* mutations were present in 34.9% (15 of 43) and 14.7% (21 of 144) in the discovery and validation cohorts, respectively, and *BRAF* mutations were present in 7.0% (3 of 43) and 5.6% (8 of 143), respectively. Only 1.1% (1 of 90) and 0.7% (1 of 146) exhibited microsatellite instability (MSI) in the discovery and validation cohorts, respectively.

Training the Molecular Subtype Classifier in Discovery Cohort

Expression data in the discovery cohort was based on whole transcriptome RNA sequencing and miRNA profiling, comprising 17,162 mRNAs and 778 miRNAs. As described in the Supplemental Methods, this was reduced to 400 mRNAs and 41 miRNAs (441 features). When training the single-layer 35 neuron neural network using 441 features, average accuracy for predicting molecular subtypes in the cross-validation testing set of the discovery cohort was 83%. After recursive feature elimination, a 31-feature signature consisting of 24 mRNAs and 7 miRNAs resulted in optimal model performance with an average accuracy of 96% across cross-validation testing sets. **eFigure 2** exhibits model performance as a function of features included in the classifier, while **eTable 1** lists the specific mRNAs and miRNAs comprising the classifier. Robustness and internal consistency of the classifier was supported by the strong concordance of predicted molecular subtypes across all 100 neural network models in this independent cohort (**eFigure 3**).

Classification of Molecular Subtypes in Validation Cohort

In the validation cohort, 73 (50%), 28 (19%), and 46 (31%) of 147 patients were classified as having canonical, immune, and stromal metastases, respectively (**eFigure 4A**). By integrated clinical-molecular risk group, 16 (11%), 25 (17%), and 103 (72%) of 144 patients were classified as having low-risk, intermediate-risk, and high-risk disease (**eFigure 4B**). Thus, there was an increase in the canonical subtype and high-risk integrated group in the validation cohort, compared to the discovery cohort. Clinical and pathologic features across molecular subtypes in the validation cohort are displayed in **eFigure 5**. Across molecular subtypes, there were no differences in the clinical or pathological features included in the CRS, tumor and nodal staging, tumor differentiation, age, or sex. The rate of positive margins (i.e. cancer present on cut surface) differed across subtypes (P=0.044). However, the incidence did not differ across subtypes in the discovery cohort (P=0.70), suggesting this did not represent a true underlying relationship.

Clinical Outcomes for Discovery and Validation Cohorts

The overall PFS and OS were highly concordant between the discovery and validation cohorts (**eFigure 6A**). Specifically, in the discovery and validation cohorts the 5-year PFS was 24.3% and 23.0% and the 5-year OS was 48.2% and 49.0%, respectively. When split by molecular subtype, there were also no significant differences in OS between discovery and validation cohorts (**eFigure 6B**). Similarly, there were no differences in OS between discovery and validation cohorts when split by integrated clinical-molecular risk group (**eFigure 6C**). Collectively, these data demonstrated strong concordance in clinical outcomes across the two cohorts by molecular subtype and integrated clinical-molecular risk group.

Prognostic Significance of Primary Tumor Gene Expression Data

The neural network classifier was also applied to the primary tumor expression data to determine whether these subtypes were also discernable in primary tumors. There was no statistically significant association between predicted molecular subtypes in primary tumors and PFS or OS (**eFigure 8**). When consensus molecular subtypes were determined for the primary tumors, there was no association between the CMS of the primary and the molecular subtype of the metastasis (**eTable 2**).[4] Finally, neither the CMS subtype of the primary tumors nor the CMS subtype of the matched liver metastases were associated with PFS and OS, though 8 (6.5%) patients with primary tumor CMS1 exhibited a trend for worse OS, consistent with prior literature (**eFigure 9**).[4] Thus, the liver metastasis molecular subtypes were prognostic when applied to liver metastasis samples (with immune subtype demonstrating superior PFS and OS), while the liver metastasis molecular subtypes applied to the primary tumors and the CMS subtypes applied to either the primaries or metastases were not.

eFigure 1
Diagram representing training and application of neural network classifier to predict molecular subtypes

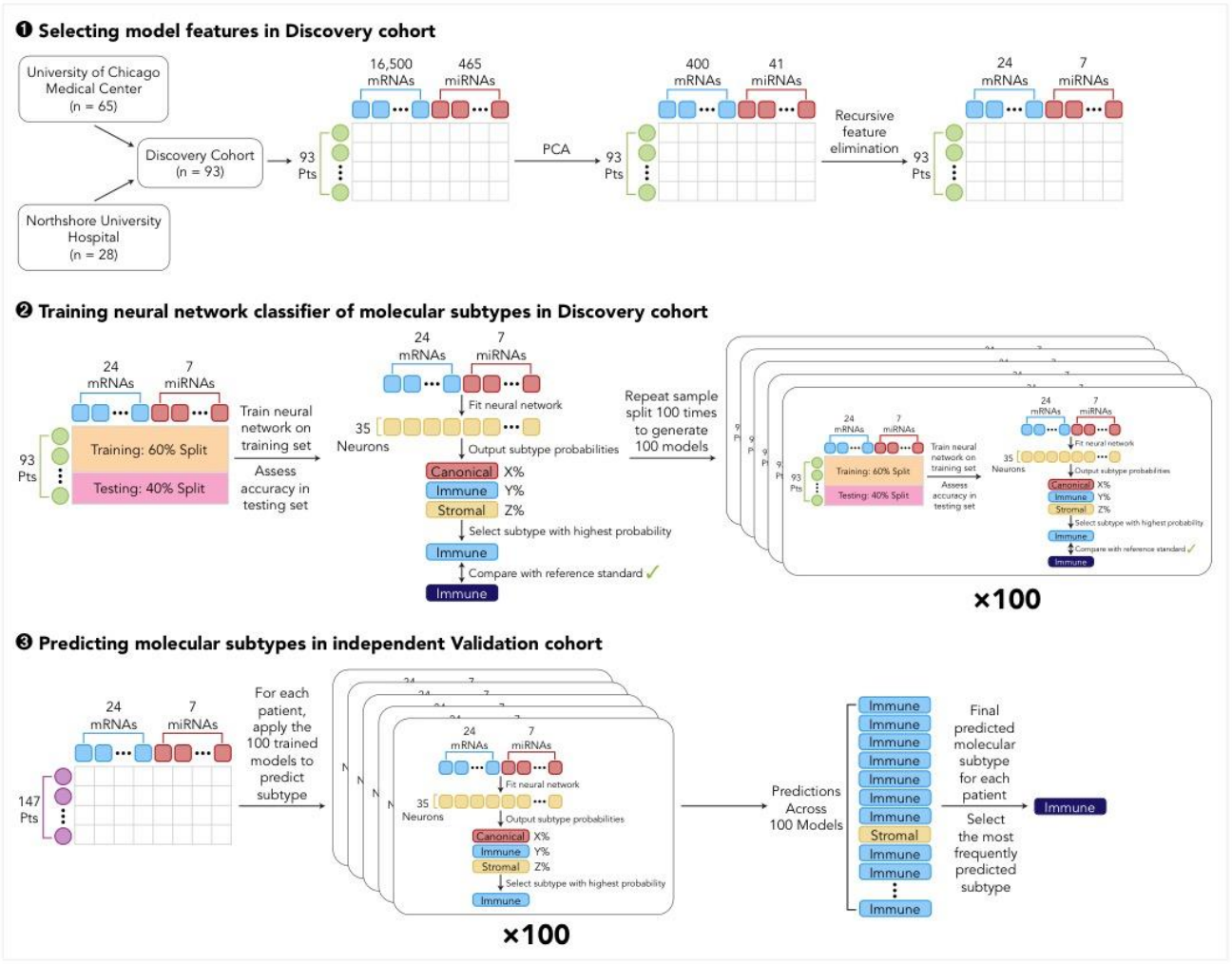

eFigure 2
Optimization of model performance (measured by the F score) as features are eliminated using recursive feature elimination

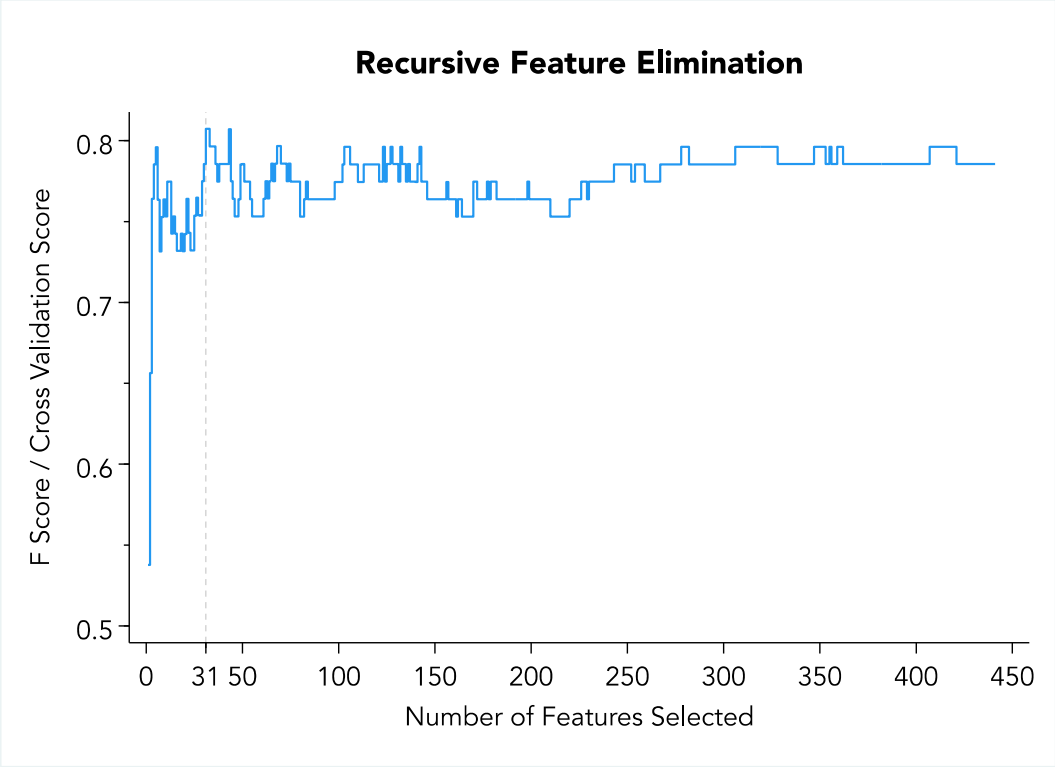

eTable 1
List of mRNAs and miRNAs included in the neural network classifier to predict molecular subtypes

Features Included in Classifier	Feature Type
JAML	mRNA
PREX2	mRNA
FAP	mRNA
MITF	mRNA
LDB2	mRNA
LRRC8C	mRNA
DDR2	mRNA
TSSC4	mRNA
CRIPT	mRNA
TCIRG1	mRNA
PKD2	mRNA
ITPR1	mRNA
ERF	mRNA
CFAP97	mRNA
RARS2	mRNA
PIK3CA	mRNA
ATAD1	mRNA
CEBPZ	mRNA
RYK	mRNA
REST	mRNA
RIF1	mRNA
USP34	mRNA
INO80D	mRNA
RBMX	mRNA
MIR548X	miRNA
MIR21	miRNA
MIR8072	miRNA
MIR762	miRNA
MIR92B	miRNA
MIR7515	miRNA
MIR30C1	miRNA

eFigure 3

Histogram representing the robustness and internal consistency of the molecular subtype classifier for liver metastases in the validation cohort. Of 100 neural network models applied for each specimen in the classifier, the distribution of model concordance for predicting molecular subtypes is visualized. *P* value corresponds to single sample T-test (N = 147) with H_a: mean percentage of concordant models across participants > 33.3% (i.e. better than a truly random classifier).

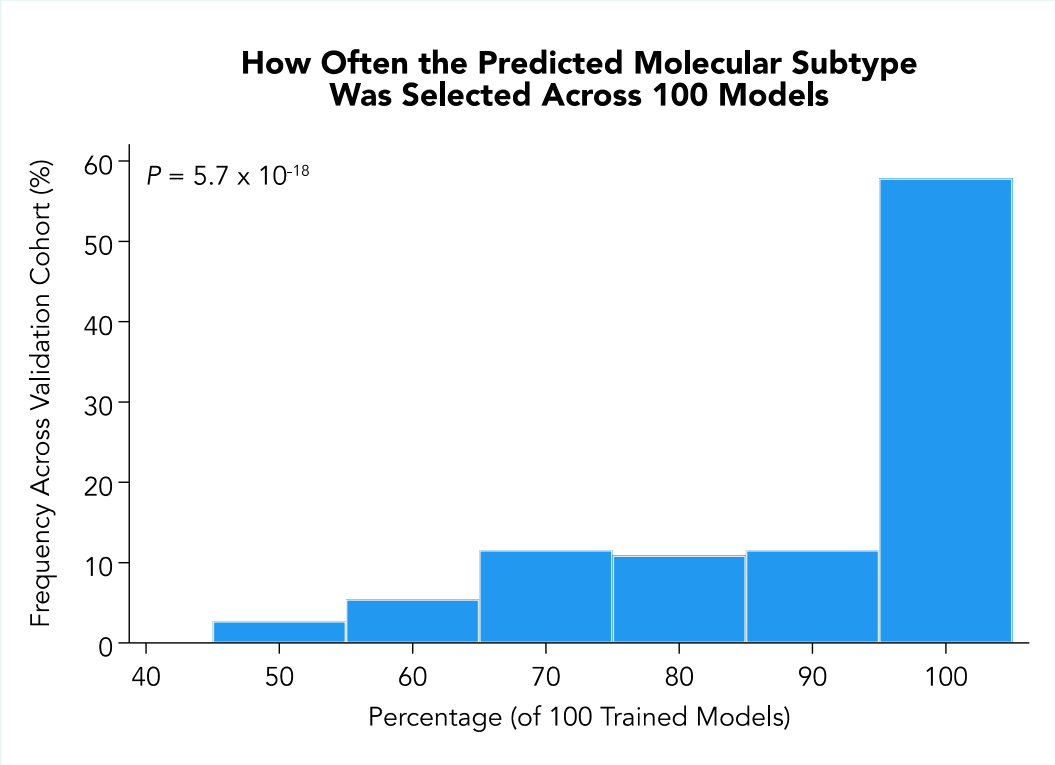

eFigure 4
Distribution of molecular subtypes and integrated clinical-molecular risk groups in the discovery and validation cohorts.

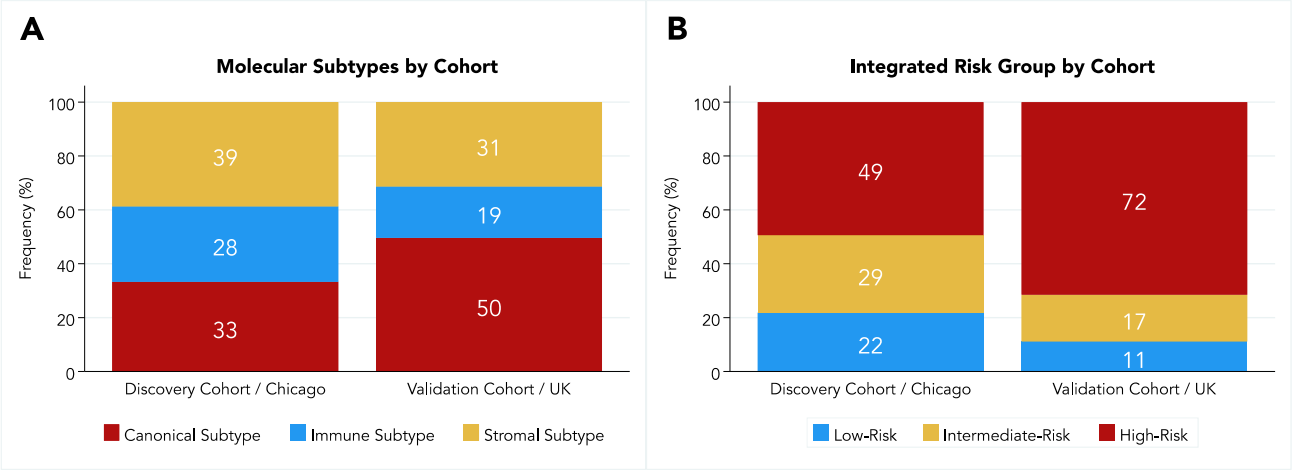

eFigure 5
Distribution of clinical and pathologic features across molecular subtypes in the validation cohort

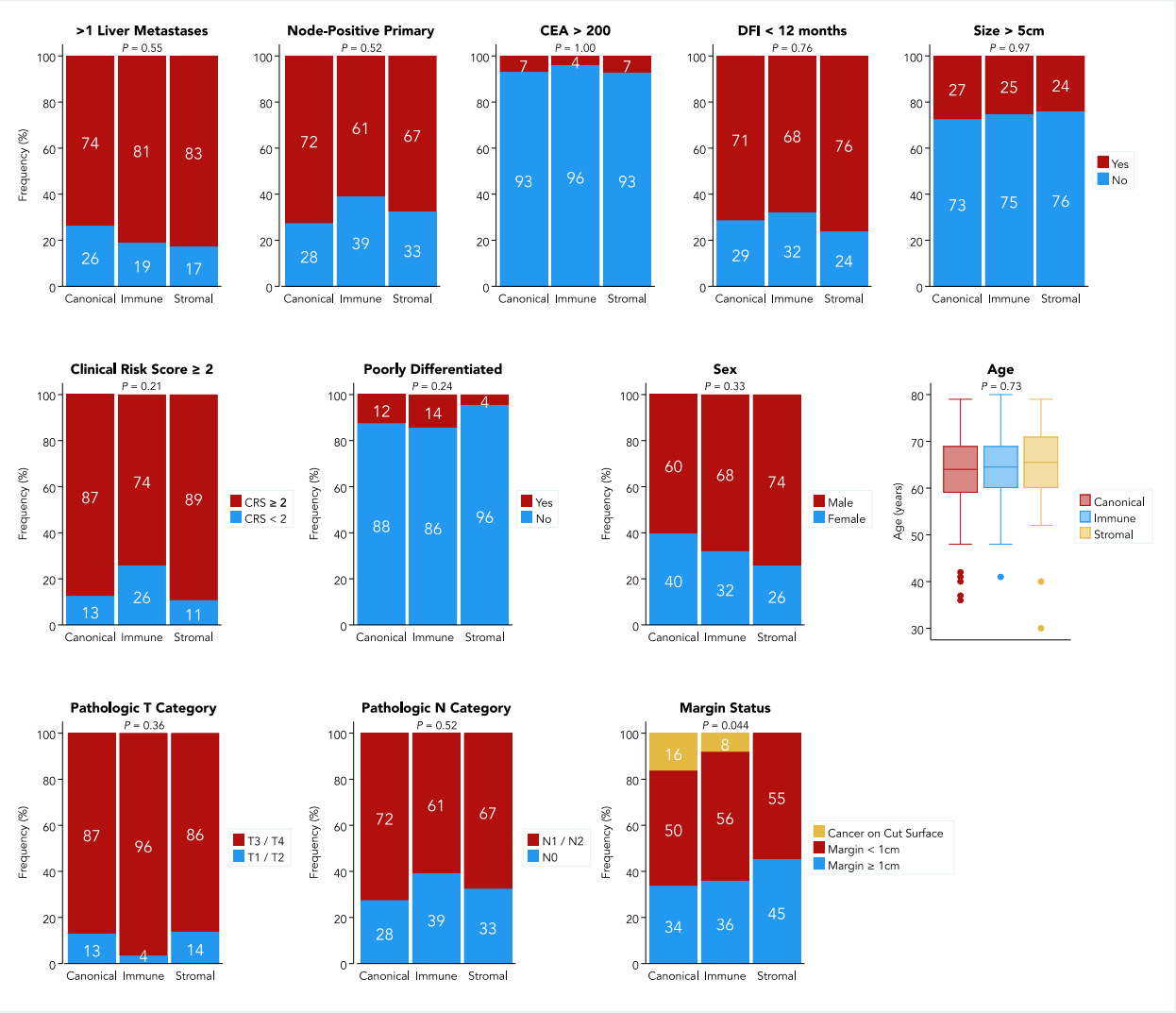

eFigure 6

(A) PFS and OS for overall discovery and validation cohorts; (B) OS for canonical, immune, and stromal subtypes; (C) OS for low-risk, intermediate-risk, high-risk integrated risk groups; X-axis represents time after surgery for the discovery cohort (in months) and time after randomization on the New EPOC trial for the validation cohort (in months)

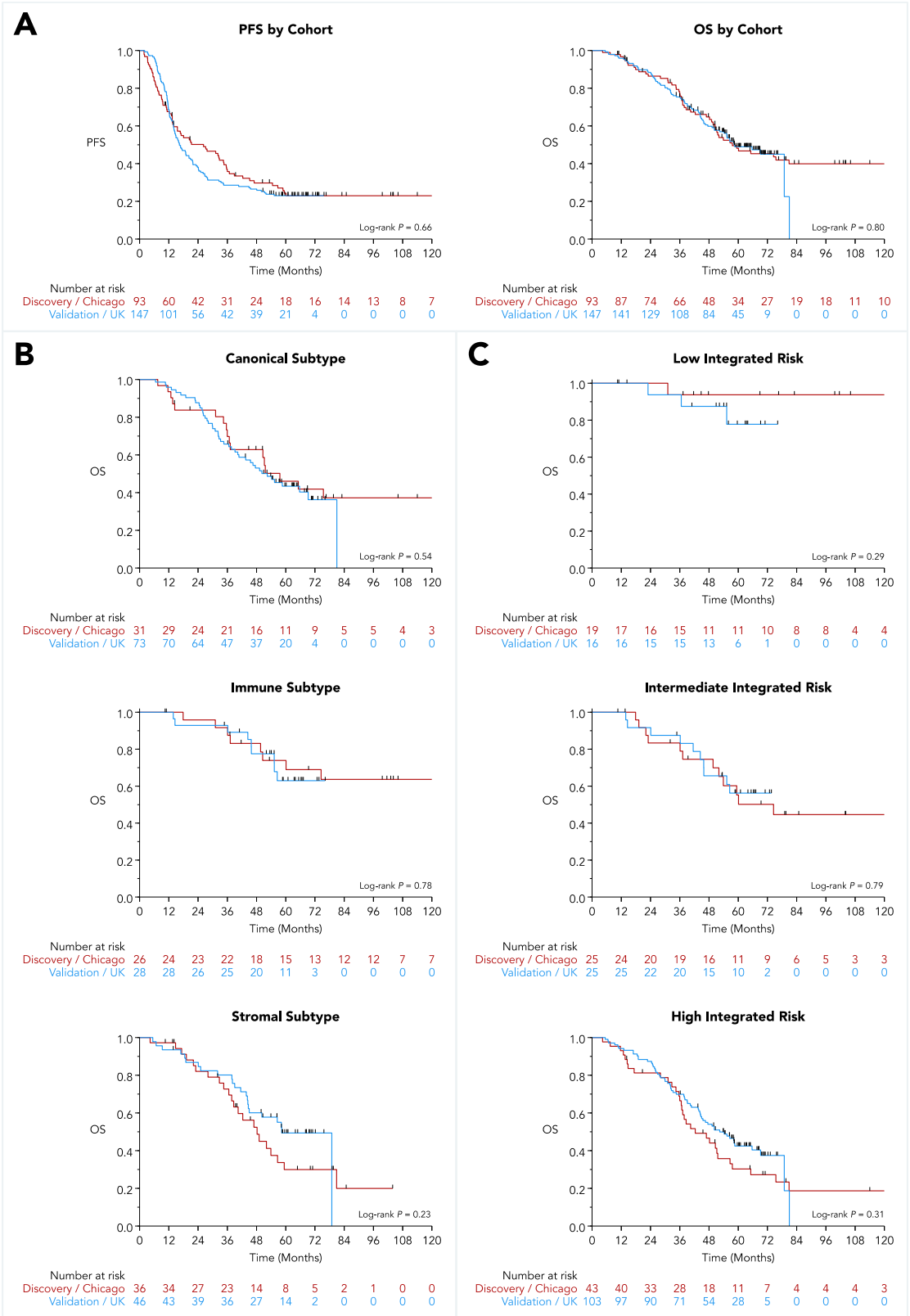

eFigure 7
Box and whisker plots for detailed visualization of (A) Single-sample gene set enrichment analysis across molecular subtypes in the validation cohort; (B) Immune deconvolution across molecular subtypes in the validation cohort

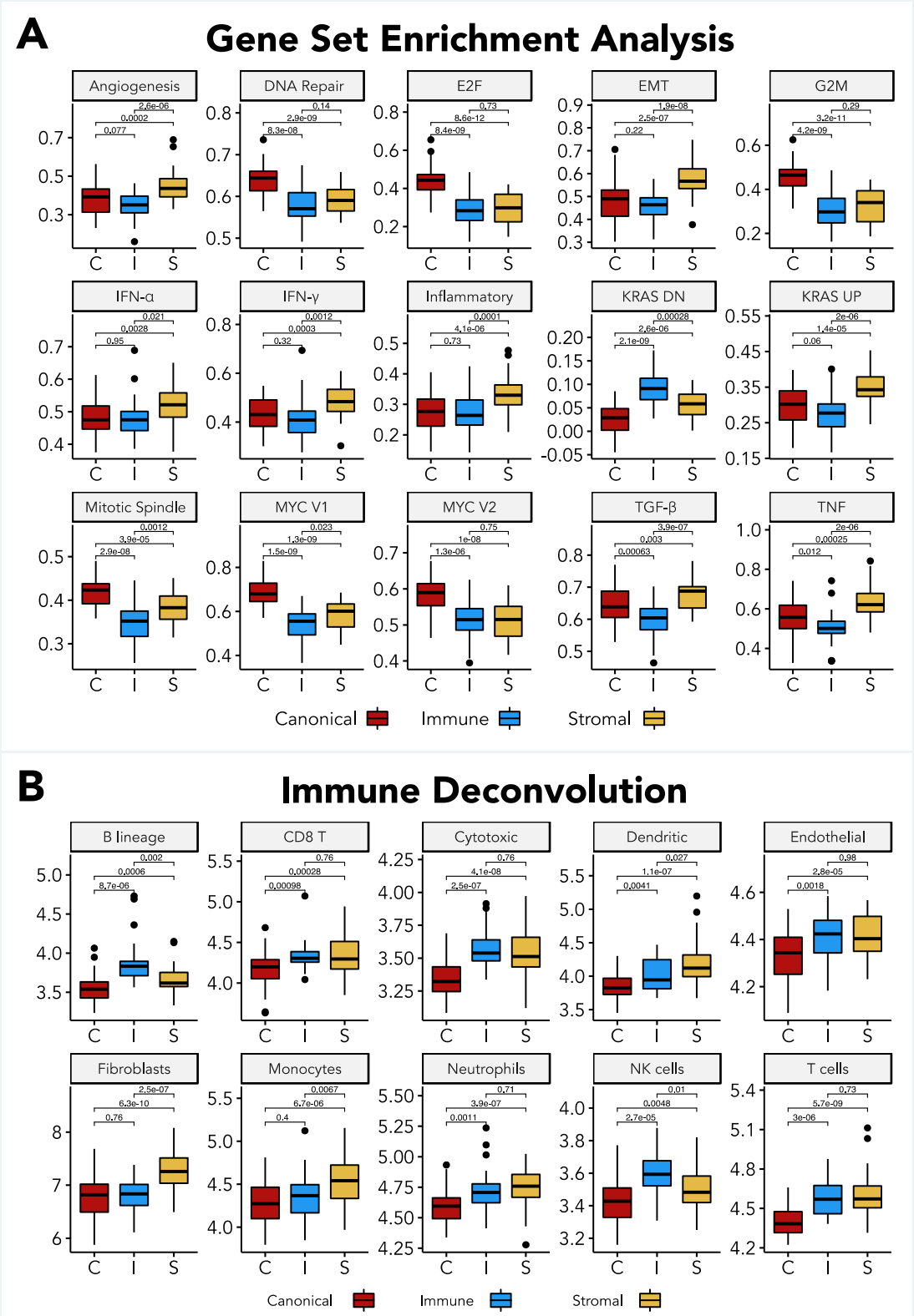

eFigure 8

Survival outcomes in validation cohort by predicted molecular subtype of primary tumor; (A) PFS; (B) OS; X-axis represents time after randomization on the New EPOC trial in months

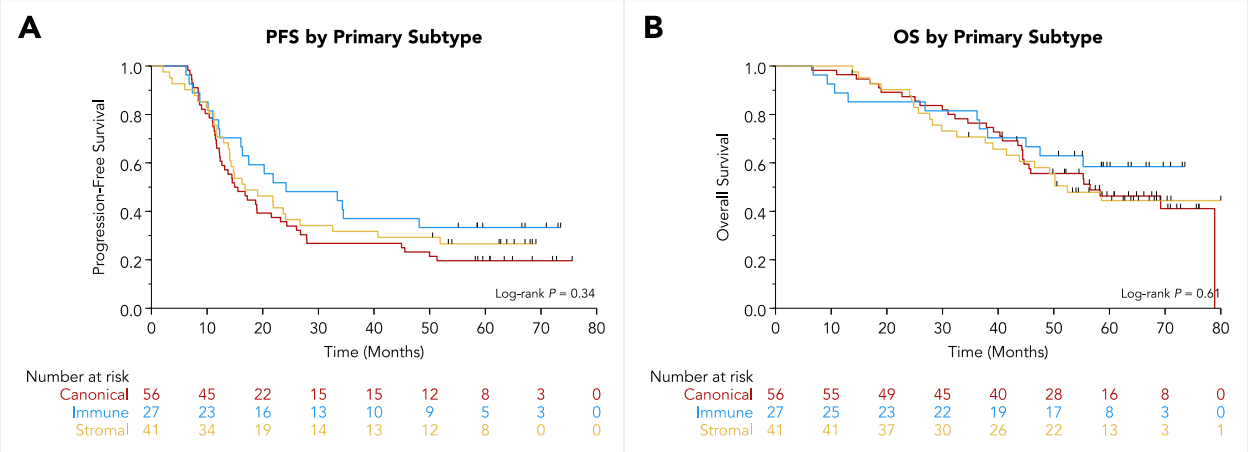

eTable 2
Association of consensus molecular subtype of the primary tumor with molecular subtype of the liver metastasis in the validation cohort

		Molecular Subtype of Metastasis			
		Canonical Subtype	**Immune Subtype**	**Stromal Subtype**	**Total**
	P = 0.37	N=59	N=27	N=38	N=124
CMS of Primary	**CMS1**	5 (62%)	2 (25%)	1 (12%)	8 (100%)
	CMS2	30 (53%)	10 (18%)	17 (30%)	57 (100%)
	CMS3	3 (33%)	4 (44%)	2 (22%)	9 (100%)
	CMS4	9 (56%)	4 (25%)	3 (19%)	16 (100%)
	Unclassified	12 (35%)	7 (21%)	15 (44%)	34 (100%)

eFigure 9

Survival outcomes in the validation cohort based on consensus molecular subtypes of either the primary tumor or liver metastasis; (A) PFS by primary tumor CMS; (B) OS by primary tumor CMS; (C) PFS by liver metastasis CMS; (D) OS by liver metastasis CMS; X-axis represents time after randomization on the New EPOC trial in months

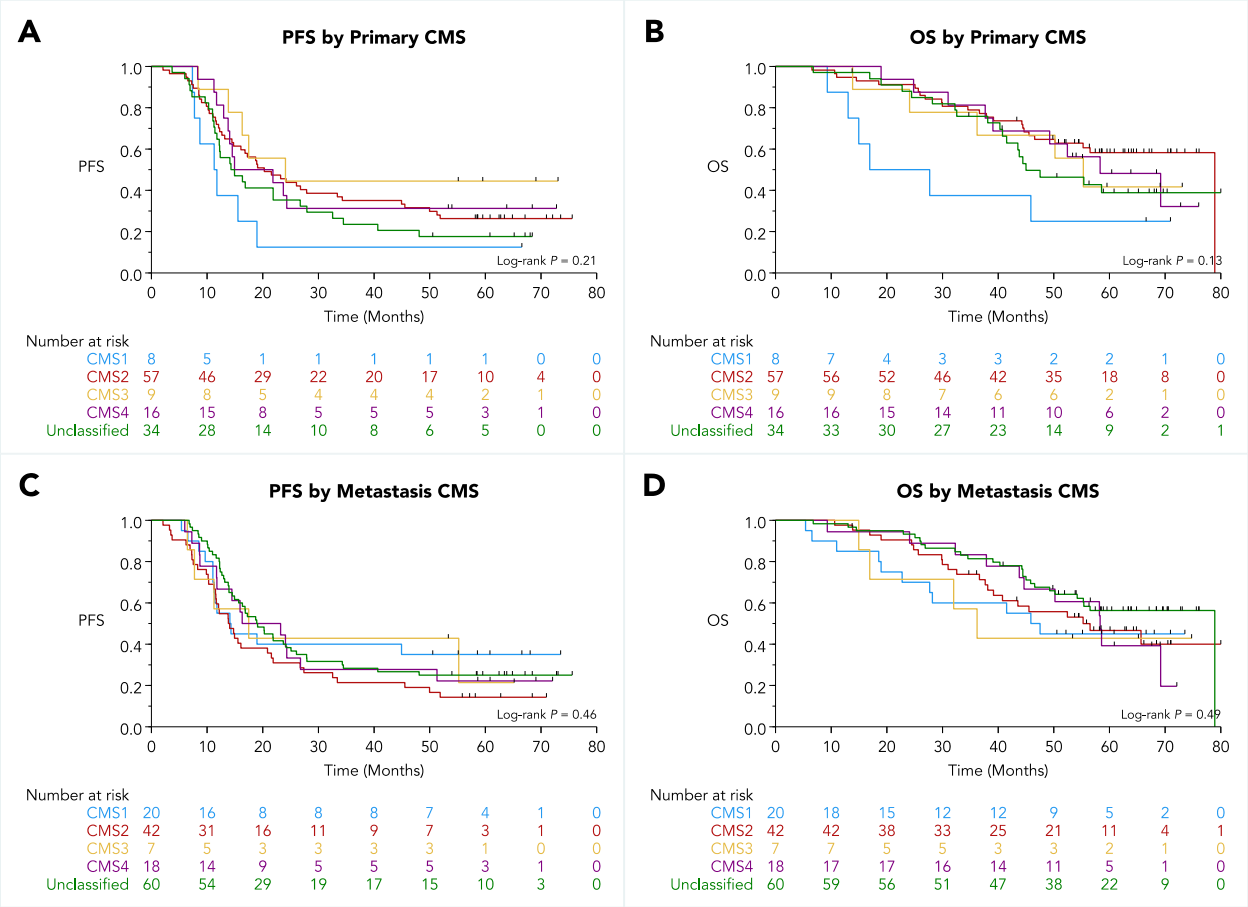

eTable 3
Sensitivity analysis demonstrating Cox proportional hazards model for PFS and OS in validation cohort, including cetuximab, age, tumor differentiation, margin status, WHO performance status, *KRAS* and *BRAF* mutation status, and primary tumor location in the model.

PFS by Molecular Subtype		
Variable	**Hazard Ratio (95% CI)**	***P***
Molecular Subtype		
Canonical	Reference	
Immune	0.43 (0.22 to 0.87)	0.018
Stromal	0.55 (0.32 to 0.92)	0.024
Clinical Risk Score		
1	Reference	
2	2.2 (1.1 to 4.5)	0.033
3	2.6 (1.3 to 5.4)	0.0090
4	2.7 (1.0 to 7.2)	0.043
5	1.7 (0.19 to 15.0)	0.63
Cetuximab		
No	Reference	
Yes	1.0 (0.64 to 1.6)	0.96
Age (years)	0.97 (0.95 to 1.0)	0.018
Tumor Differentiation		
Well/Moderate	Reference	
Poor	1.8 (0.85 to 3.8)	0.12
Shortest Margin Between Cancer and Cut Surface		
Margin ≥ 1cm	Reference	
Margin < 1cm	1.0 (0.60 to 1.7)	>0.99
No Margin (Cancer Visible on Cut Surface)	1.4 (0.61 to 3.3)	0.42
WHO Performance Status		
0	Reference	
1	1.3 (0.76 to 2.1)	0.36
KRAS Mutant		

Wildtype	Reference	
Mutant	1.3 (0.65 to 2.6)	0.46
BRAF Mutant		
Wildtype	Reference	
Mutant	0.88 (0.36 to 2.2)	0.78
Primary Tumor Location		
Right Colon	Reference	
Left Colon	0.59 (0.28 to 1.3)	0.17
Rectum	0.64 (0.32 to 1.3)	0.20
Recto-Sigmoid	0.62 (0.29 to 1.3)	0.21
Other	0.98 (0.47 to 2.0)	0.96
OS by Molecular Subtype		
Variable	**Hazard Ratio (95% CI)**	***P***
Molecular Subtype		
Canonical	Reference	
Immune	0.44 (0.18 to 1.1)	0.082
Stromal	0.75 (0.39 to 1.4)	0.38
Clinical Risk Score		
1	Reference	
2	1.6 (0.57 to 4.7)	0.36
3	2.6 (0.95 to 7.2)	0.064
4	2.4 (0.72 to 7.8)	0.16
5	0.69 (0.07 to 7.1)	0.75
Cetuximab		
No	Reference	
Yes	2.0 (1.2 to 3.5)	0.014
Age (years)	0.99 (0.97 to 1.0)	0.66
Tumor Differentiation		
Well/Moderate	Reference	
Poor	1.0 (0.37 to 2.7)	0.98
Shortest Margin Between Cancer and Cut Surface		

Margin ≥ 1cm	Reference	
Margin < 1cm	0.84 (0.45 to 1.6)	0.58
No Margin (Cancer Visible on Cut Surface)	2.4 (0.96 to 5.9)	0.060
WHO Performance Status		
0	Reference	
1	1.6 (0.88 to 3.0)	0.12
KRAS Mutant		
Wildtype	Reference	
Mutant	1.9 (0.92 to 4.1)	0.083
BRAF Mutant		
Wildtype	Reference	
Mutant	1.3 (0.48 to 3.6)	0.58
Primary Tumor Location		
Right Colon	Reference	
Left Colon	1.3 (0.54 to 2.9)	0.60
Rectum	0.61 (0.26 to 1.4)	0.25
Recto-Sigmoid	0.69 (0.27 to 1.8)	0.44
Other	0.99 (0.43 to 2.3)	0.97
PFS by Integrated Risk		
Variable	**Hazard Ratio (95% CI)**	***P***
Integrated Risk		
Low	0.34 (0.16 to 0.71)	0.0042
Intermediate	0.59 (0.32 to 1.1)	0.091
High	Reference	
Cetuximab		
No	Reference	
Yes	1.0 (0.67 to 1.5)	0.95
Age (years)	0.97 (0.96 to 1.0)	0.020
Tumor Differentiation		
Well/Moderate	Reference	
Poor	1.5 (0.75 to 3.0)	0.26

Shortest Margin Between Cancer and Cut Surface		
Margin ≥ 1cm	Reference	
Margin < 1cm	1.1 (0.68 to 1.7)	0.74
No Margin (Cancer Visible on Cut Surface)	1.4 (0.66 to 3.0)	0.38
WHO Performance Status		
0	Reference	
1	1.5 (0.96 to 2.4)	0.072
KRAS Mutant		
Wildtype	Reference	
Mutant	1.5 (0.84 to 2.8)	0.17
BRAF Mutant		
Wildtype	Reference	
Mutant	1.0 (0.42 to 2.5)	0.96
Primary Tumor Location		
Right Colon	Reference	
Left Colon	0.68 (0.34 to 1.36)	0.28
Rectum	0.84 (0.43 to 1.7)	0.62
Recto-Sigmoid	0.67 (0.33 to 1.4)	0.28
Other	1.1 (0.58 to 2.2)	0.73
OS by Integrated Risk		
Variable	**Hazard Ratio (95% CI)**	***P***
Integrated Risk		
Low	0.28 (0.08 to 0.92)	0.036
Intermediate	0.72 (0.33 to 1.6)	0.41
High	Reference	
Cetuximab		
No	Reference	
Yes	1.8 (1.1 to 3.0)	0.021
Age (years)	0.99 (0.97 to 1.0)	0.56
Tumor Differentiation		

Well/Moderate	Reference	
Poor	1.1 (0.43 to 2.6)	0.89
Shortest Margin Between Cancer and Cut Surface		
Margin ≥ 1cm	Reference	
Margin < 1cm	0.82 (0.46 to 1.5)	0.51
No Margin (Cancer Visible on Cut Surface)	2.1 (0.97 to 4.7)	0.060
WHO Performance Status		
0	Reference	
1	1.9 (1.1 to 3.3)	0.016
KRAS Mutant		
Wildtype	Reference	
Mutant	2.2 (1.1 to 4.3)	0.021
BRAF Mutant		
Wildtype	Reference	
Mutant	1.4 (0.51 to 3.7)	0.53
Primary Tumor Location		
Right Colon	Reference	
Left Colon	1.1 (0.50 to 2.5)	0.79
Rectum	0.63 (0.28 to 1.4)	0.27
Recto-Sigmoid	0.75 (0.31 to 1.8)	0.53
Other	1.0 (0.46 to 2.3)	0.96

References

1. Pitroda SP, Khodarev NN, Huang L, et al. Integrated molecular subtyping defines a curable oligometastatic state in colorectal liver metastasis. *Nat Commun*. 2018;9(1):1793. doi:10.1038/s41467-018-04278-6

2. Bridgewater JA, Pugh SA, Maishman T, et al. Systemic chemotherapy with or without cetuximab in patients with resectable colorectal liver metastasis (New EPOC): long-term results of a multicentre, randomised, controlled, phase 3 trial. *The Lancet Oncology*. 2020;21(3):398-411. doi:10.1016/S1470-2045(19)30798-3

3. Primrose J, Falk S, Finch-Jones M, et al. Systemic chemotherapy with or without cetuximab in patients with resectable colorectal liver metastasis: the New EPOC randomised controlled trial. *The Lancet Oncology*. 2014;15(6):601-611. doi:10.1016/S1470-2045(14)70105-6

4. Guinney J, Dienstmann R, Wang X, et al. The consensus molecular subtypes of colorectal cancer. *Nat Med*. 2015;21(11):1350-1356. doi:10.1038/nm.3967

5. Barbie DA, Tamayo P, Boehm JS, et al. Systematic RNA interference reveals that oncogenic KRAS-driven cancers require TBK1. *Nature*. 2009;462(7269):108-112. doi:10.1038/nature08460

6. Becht E, Giraldo NA, Lacroix L, et al. Estimating the population abundance of tissue-infiltrating immune and stromal cell populations using gene expression. *Genome Biol*. 2016;17(1):218. doi:10.1186/s13059-016-1070-5

7. Fong Y, Fortner J, Sun RL, Brennan MF, Blumgart LH. Clinical score for predicting recurrence after hepatic resection for metastatic colorectal cancer: analysis of 1001 consecutive cases. *Ann Surg*. 1999;230(3):309-318; discussion 318-321. doi:10.1097/00000658-199909000-00004